

The dynamics of conformational isomerization in flexible biomolecules. I. Hole-filling spectroscopy of N-acetyl tryptophan methyl amide and N-acetyl tryptophan amide

Brian C. Dian, Asier Longarte, Paul R. Winter, and Timothy S. Zwier^{a)}

Department of Chemistry, 560 Oval Drive, Purdue University, West Lafayette, Indiana 47907-2084

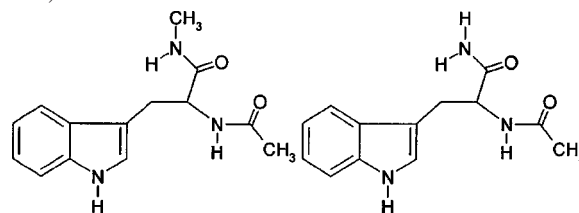
(Received 6 August 2003; accepted 26 September 2003)

The conformational isomerization dynamics of N-acetyl tryptophan methyl amide (NATMA) and N-acetyl tryptophan amide (NATA) have been studied using the methods of IR-UV hole-filling spectroscopy (HFS) and IR-induced population transfer spectroscopy (IR-PTS), which were developed for this purpose. Single conformations of these molecules were selectively excited in well-defined NH stretch fundamentals. This excess energy was used to drive conformational isomerization. By carrying out the infrared excitation early in a supersonic expansion, the excited molecules were recooled into their zero-point levels, partially refilling the hole created in the ground state population of one of the conformers, and creating gains in population in other conformers. These changes in population were detected using laser-induced fluorescence downstream in the expansion. In HFS, the IR wavelength is fixed and the UV laser tuned in order to determine where the population went following selective infrared excitation. In IR-PTS, the UV is fixed to monitor the population of a given conformation, and the IR is tuned to record the IR-induced changes in the population of the monitored conformer. Besides demonstrating the capability of the experiment to change the downstream conformational population distribution, the IR-PTS scans were used to extract two quantitative results: (i) The fractional populations of the conformers in the absence of the infrared, and (ii) the isomerization quantum yields for each of the six unique amide NH stretch fundamentals (three conformers each with two amide groups). The method for obtaining quantum yields is described in detail. In both NATMA and NATA, the quantum yields show modest conformational specificity, but only a hint of vibrational mode specificity. The prospects for the hole-filling technique for providing insight into energy flow in large molecules are discussed, leaving a more detailed theoretical modeling to the adjoining paper [Evans *et al.*, *J. Chem. Phys.* **120**, 148 (2004)]. © 2004 American Institute of Physics. [DOI: 10.1063/1.1626540]

I. INTRODUCTION

Studies of conformational isomerization have typically occurred in one of two size regimes. At one extreme, isomerization occurs on a potential energy surface with two conformational minima (e.g., *cis/trans* isomerization) that are connected by a single transition state along a well-defined reaction coordinate. In such circumstances, detailed state-to-state studies are often possible that probe the reaction energetics, time scales, and pathways on the potential energy surface in significant detail.^{1–3} In the other extreme are large macromolecules, such as proteins, that have potential energy landscapes that are staggeringly complex, so that the nature of the unfolded “reactant” and folded “product,” the pathway(s) that connect them, and the time scales over which reactions occur are difficult to define, determine, or control.^{4,5} Between these two extremes lies an interesting size regime in which the full set of conformational minima can still be enumerated and single conformations selectively excited and interrogated, but yet the complexity of the potential energy surface is sufficient to raise issues that may carry through to much larger molecules.

We have recently reported results from an experimental method that is designed to probe the dynamics of conformational isomerization of flexible molecules in this intermediate size regime.⁶ The method has been applied first to the methyl-capped dipeptide N-acetyl tryptophan methyl amide (NATMA) and its close analog N-acetyl tryptophan amide (NATA) shown below.



To illustrate the level of conformational complexity inherent to these molecules, it is helpful to summarize the results of a recent exhaustive search of the potential energy landscape of NATMA using the AMBER force field.⁷ This landscape will be discussed in greater detail in the adjoining paper (Ref. 10). According to the AMBER force field, NATMA possesses 164 conformational minima, about 60 of which are within 10 kcal/mol of the global minimum. There are 714 transition states connecting these 164 minima.⁷ The potential energy landscape divides into subregions separated

^{a)}Electronic mail: zwier@perdue.edu

by the rather large barriers (15–20 kcal/mol) associated with *cis*–*trans* isomerization of the two amide groups in the molecule. Not surprisingly, the low-energy minima of NATMA have both amide groups in the *trans* configuration. All of these low-energy minima fall into one of two conformational families: (i) C5 structures with an extended dipeptide backbone, and C7_{eq} structures in which an intramolecular H bond is formed between the methyl amide NH group and the N-acetyl carbonyl oxygen, forming a seven-membered H-bonded ring. This seven-membered ring is equivalent to a γ -turn in longer polypeptides.

The present study of conformational isomerization dynamics builds off a foundation of IR and UV spectroscopy on gas-phase NATMA and NATA cooled in a supersonic expansion, which has been reported in this journal recently.⁷ The double resonance methods of fluorescence-dip IR (FDIR) spectroscopy and UV–UV hole-burning spectroscopy have been used to record IR and UV spectra of single conformations of NATMA and NATA free from interference from one another. Such studies establish the conformational preferences of the isolated molecule free from solvent, providing results against which force field and *ab initio* calculations can be compared.

Armed with assignments of the conformations present in the expansion and their IR spectral signatures, we have probed the dynamics of conformational isomerization following the excitation of single conformations in well-defined vibrational modes. This work employs two closely related methods: IR–UV hole-filling spectroscopy (HFS) and IR-induced population transfer spectroscopy (IR-PTS). Both methods employ a conceptually simple but powerful modification to the hole-burning and fluorescence-dip spectroscopy experiments.

The FDIR spectra of NATMA and NATA were recorded with the IR and UV laser beams spatially overlapped in the collision-free region of the supersonic expansion.⁷ The spectra show that the amide NH stretch fundamentals of the individual conformations are adequately separated from one another to enable selective excitation of a single amide NH stretch fundamental of a particular conformation of the molecule of interest. By moving the IR laser upstream to just outside the expansion orifice, selective excitation of a single conformation in a well-defined NH stretch fundamental can still be achieved, creating a “hole” in the ground-state population of one of the conformers. However, the excited conformers now possess 10 kcal/mol of energy (3500 cm⁻¹) not available to the other conformers, and they can use this energy to undergo conformational isomerization. In order to complete the isomerization process and enable conformation-specific detection, collisional cooling of this excited population is used either to repopulate the same minimum, or isomerize and cool the molecule into other conformational zero-point levels. The change in population of each of the conformers is then detected downstream in the expansion using laser-induced fluorescence. As we shall see, HFS detects where the population went, while population transfer spectroscopy quantitatively measures the fractional population change in each conformation as a function of IR wavelength.

In the present article, we give a complete description of the experimental methods of HFS and population transfer spectroscopy, applied to NATMA and then extended to its close analog NATA. The present data on the isomerization dynamics of NATMA and NATA are so closely connected with the spectroscopy of these molecules that a brief review of that spectroscopy is critical to an understanding of the dynamics studies. This is given in Sec. II. Sections III and IV provide details of the experimental methods and give an overview of the key results. The approach used to extract fractional populations and isomerization quantum yields is described in some detail in Sec. V. Data sets extending over a wider range of conditions have provided key tests of aspects of the methods, and have led to a refinement in the experimental protocol and analysis for extracting isomerization quantum yields from each of the NH stretch fundamentals of individual conformations of NATMA and NATA. A scheme for visualizing and interpreting the isomerization quantum yields is presented in Sec. VI, and used to present the isomerization quantum yields for both NATMA and NATA. These quantum yields show modest conformation specificity, and only hints of vibrational mode specificity. Finally, the general implications of these results for isomerization and energy flow in large molecules are discussed in Sec. VII, leaving a more detailed theoretical modeling of the isomerization dynamics to the adjoining paper (Ref. 10).

II. OVERVIEW OF THE SPECTROSCOPY OF N-ACETYL TRYPTOPHAN METHYL AMIDE AND N-ACETYL TRYPTOPHAN AMIDE

The essential elements of the UV and IR spectroscopy of NATMA and NATA are summarized here. The reader is referred to Ref. 7 for a complete description of this spectroscopy and the process used to assign the spectra of individual conformations to particular conformational isomers.

Figure 1 presents the LIF spectrum of NATMA [Fig. 1(a)] and a series of UV–UV hole-burning spectra [Figs. 1(b)–1(d)] that prove that there are three conformations of NATMA with significant population downstream in the expansion. The hole-burning spectra establish which transitions in the LIF spectrum can be assigned to which conformer, thereby providing the UV spectrum of each conformation free from interference from the others present in the expansion. Similar hole-burning studies of NATA (not shown) identified contributions to the laser-induced fluorescence (LIF) spectrum from only two conformations. In both NATA and NATMA, it is the C7_{eq} conformer that produces the congested vibronic structure, while the C5 conformers possess sharp well-resolved vibronic structure. The unique UV spectra of the C7_{eq} conformers has been ascribed to a reordering of the electronic states induced by the C7_{eq}(ΦP) dipeptide backbone conformation.⁸

The hole-burning spectra (Fig. 1) were used to select UV wavelengths where fluorescence due to each of the three conformers of NATMA (labeled A, B, and C) could be selectively monitored. These UV wavelengths were then used to record IR spectra of each of the conformations, using FDIR spectroscopy. In order to make conformational assignments, the FDIR spectra were compared with the harmonic vibra-

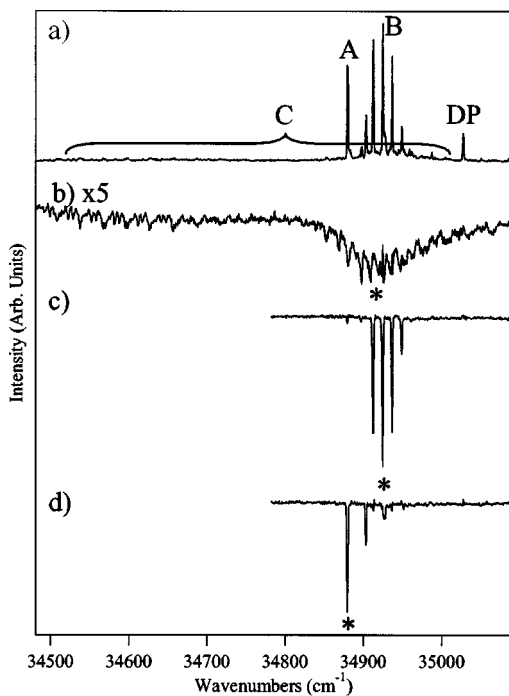


FIG. 1. (a) LIF excitation spectrum of NATMA in the region of the S_0-S_1 origin. (b)–(d) UV-UV hole-burning scans while hole-burning on the transitions marked by an asterisk. The hole-burning scans prove that there are three conformations of NATMA, and determine the UV transitions assignable to each. (Figure adapted from Ref. 7.)

tional frequencies and IR intensities of the low-energy conformational minima calculated using a range of *ab initio* and density functional theory methods. This analysis led to the assignments for the conformations of NATMA and NATA summarized in Fig. 2.

Figures 3(a) and 3(b) present overlaid sets of FDIR spectra for NATMA and NATA, respectively, in the NH stretch region. The point of overlaying the spectra in this way is to highlight the unique IR spectral signatures of the individual

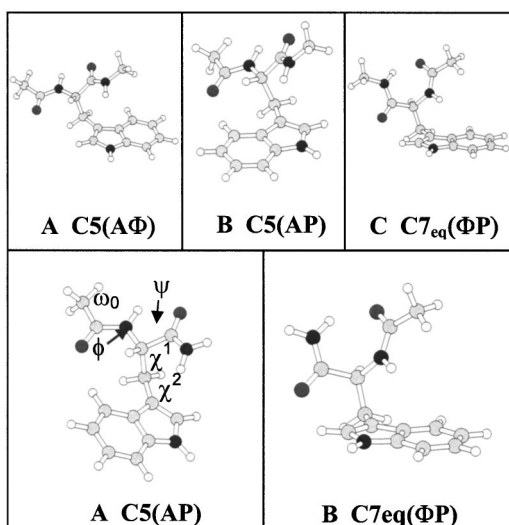


FIG. 2. Assigned structures of the experimentally observed conformational minima of NATMA (a)–(c) and NATA [(d) and (e)]. (The nomenclature used is taken from Ref. 7.) The ϕ and ψ designations on the NH bonds refer to the Ramachandran angles of the dipeptide backbone.

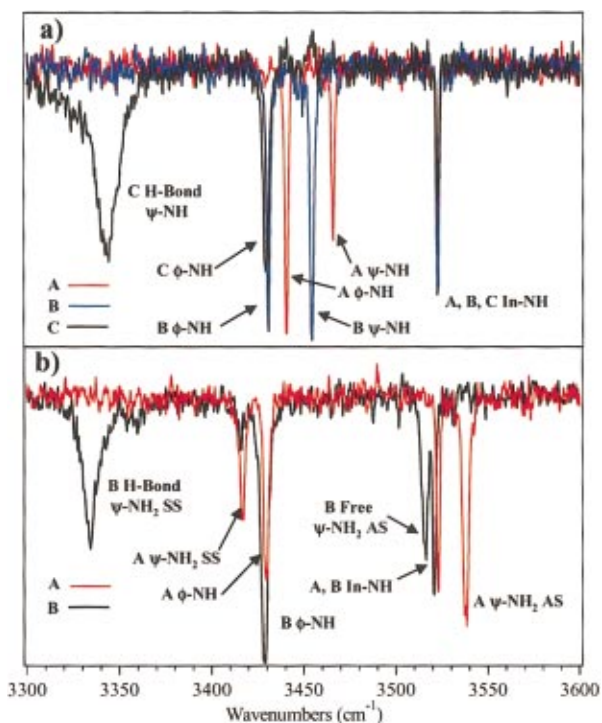


FIG. 3. (Color) The series of FDIR spectra of (a) conformers A–C of NATMA, and (b) conformers A and B of NATA, in the NH stretch region. The overlaid spectra highlight the unique IR frequencies of the amide NH stretch fundamentals of the single conformations that would enable selective excitation of a single conformation in a well-defined NH oscillator. The indole NH stretch (3523 cm^{-1}) is unchanged in frequency with dipeptide conformation, making selective excitation impossible in that case.

conformations of these molecules. All conformers possess indole NH stretch fundamentals that are essentially unchanged in wave number position (3523 cm^{-1}) from one another. This is not surprising given the isolation of the indole NH bond from the dipeptide backbone responsible for the various conformations. The other NH stretch transitions are due to the two amide groups present in the dipeptide backbone. These are much more sensitive to conformational changes. The $C7_{eq}$ structures show an N-terminal amide NH stretch fundamental that is shifted down in frequency about 100 cm^{-1} relative to the corresponding band in the $C5$ spectra. This band is also increased in intensity and broadened due to formation of the intramolecular H bond. All the other amide NH stretch bands in NATMA are found in the $3430\text{--}3470\text{ cm}^{-1}$ region, and have small but characteristic shifts from one conformation to the next. In NATA, the NH_2 group produces symmetric and antisymmetric NH stretch fundamentals that are separated by 120 cm^{-1} .

The infrared spectra in Fig. 3 suggested to us that selective IR excitation early in the supersonic expansion could be used to study the dynamics of conformational isomerization on a conformation-specific and vibrationally mode selective basis. It is clear from the spectra of Fig. 3(a) that it should be possible to selectively excite one of the conformers of NATMA without exciting the other two, simply by proper choice of IR wavelength. For example, excitation at 3440 or 3466 cm^{-1} would selectively excite conformer A, while B could be excited at 3454 cm^{-1} , or C at 3340 cm^{-1} . Selective

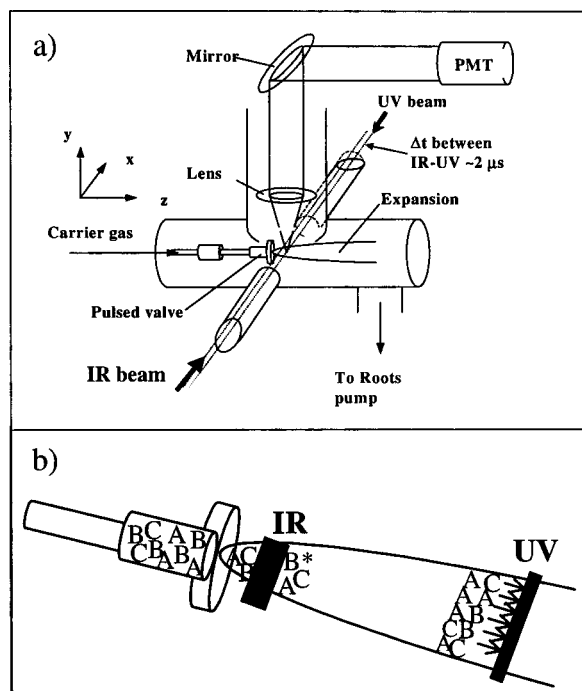


FIG. 4. Schematic diagram of (a) the experimental apparatus and (b) laser beam positions used in IR HFS and IR-PTS. Selective IR excitation of a single conformation is carried out early in the supersonic expansion, followed by collisional recoiling either back into the original minimum or into other minima following isomerization. The changes in conformational population are detected downstream using LIF. In HFS, the IR (10 Hz) is held fixed at a given wavelength while the UV (20 Hz) is tuned. In IR-PTS, the IR is tuned while the UV is held fixed at a unique wavelength where a single conformer absorbs. In either case, the difference in fluorescence signal with and without the IR laser is detected downstream.

excitation of a single conformation in a well-defined NH stretch oscillator gives that conformation about 3500 cm^{-1} ($\sim 10 \text{ kcal/mol}$) of energy that the other conformers do not possess. This is enough energy to overcome many of the barriers that separate conformational minima; hence, the IR excitation can be used to drive conformational isomerization. By exciting early in the supersonic expansion, one can cool the excited molecules to their conformational zero-point levels prior to interrogation with the ultraviolet laser downstream.

III. EXPERIMENT

Figure 4 shows a schematic diagram of the experimental apparatus and laser configuration used for these studies, while Fig. 5 illustrates the methods via energy level and timing diagrams. Solid samples of NATMA and NATA are heated to temperatures of 150–160 °C and entrained in a flow of helium at a backing pressure of about 6 bar. A pulsed valve operating at 20 Hz (General Valve, Fairfield, NJ, 800 μm diameter) is used to cool the molecules into their conformational zero-point levels in a supersonic free jet expansion. Total flow rates of about 150 standard cm^3/min in a 1.0–1.5 ms long gas pulse are typically used. These large flows are helpful in maximizing LIF signal from NATMA and NATA, while minimizing the thermal decomposition of the sample.

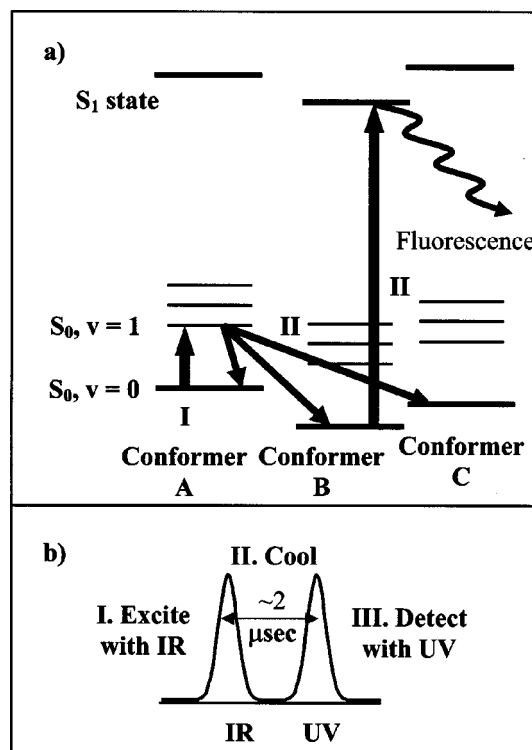


FIG. 5. (a) Schematic energy level diagram and (b) timing diagram for HFS and IR-PTS. The case of selective IR excitation of conformer A is shown.

The IR output of an IR parametric converter (LaserVision, Bellevue, WA) crosses the expansion 1.5–3 nozzle diameters downstream from the expansion orifice (i.e., $x/D = 1.5-3$). The IR beam is focused with a 50 cm focal length CaF_2 lens resulting in a final beam diameter of slightly less than 1 mm. Quantitative measurements were usually taken at $x/D = 2.5$. Based on LIF spectra recorded at this distance, hot band intensities can be used to estimate a vibrational temperature of about 10–15 K at the point of IR excitation. IR pulse energies are typically chosen so as to effect significant fractional population depletion in the absence of hole-filling collisions (30%–60% depletion).

The doubled output of a Nd:YAG-pumped dye laser is used for LIF detection. The central portion of the UV beam ($\sim 2 \text{ mm}$ diameter) is selected for passage through the vacuum chamber, which is then focused with a 70 cm focal length S1UV lens resulting in a final beam diameter of about 0.5 mm inside the vacuum chamber. This beam size is chosen to ensure that the molecules detected in LIF are inside a bigger volume of IR excited molecules. This is easily checked by changing the timing between the two lasers to view the fall off in signal on either side of the best overlap position. Under typical hole-filling conditions, the UV beam is positioned at $x/D \sim 7$, with a timing delay between IR and UV laser pulses of about $2 \mu\text{s}$. We estimate that the IR excited molecules undergo thousands of collisions with helium between IR excitation and detection.

In order to detect only the changes induced by the IR laser, the difference in fluorescence signal was recorded using the active baseline subtraction mode of our gated integrator (SRS 250, Sunnyvale, CA). The infrared laser (10 Hz)

is pulsed every other time the UV laser fires (20 Hz). A negative (positive) signal indicates a depletion (gain) in the fluorescence signal.

Two types of spectra can be recorded, depending on whether the IR or the UV laser is tuned. In IR-UV HFS, the IR laser is held fixed at a wavelength where selective IR excitation of a single conformer can be carried out. The UV laser is then tuned through the transitions of interest in the LIF spectrum. Dips in population will be seen as depletions in the LIF spectrum, while gains in population will produce positive-going signals. As a result, IR-UV HFS can be used to determine *where the population went* following IR excitation of a single conformer.

Alternatively, IR-induced population transfer spectroscopy (IR-PTS) detects *the population changes induced in a single conformer by infrared excitation*. As it turns out, this form is the more useful of the two for extracting quantitative data on the isomerization process. In IR-PTS, the UV laser is fixed on a vibronic transition in the LIF spectrum ascribable to a particular conformer. The magnitude of the LIF signal is directly proportional to the ground-state population of that conformer. As the IR source is tuned, IR transitions due to that conformer will show depletions in the LIF signal, while transitions that pump population out of other conformations into the one probed will lead to gains in the signal. By setting up the gated integrator output to have a known signal level in the absence of the infrared (e.g., 6 V output on a 0–10 V scale), the active baseline subtraction signal can be divided by this total signal level to obtain fractional population changes.

The application of these methods to NATMA and NATA is complicated by the fact that these molecules each have a C_{7eq} conformation [NATMA (C) and NATA (B)] that produces a broad and highly congested LIF spectrum [Fig. 1(b) for NATMA] that extends underneath the strong vibronic transitions due to the C5 conformer(s). As a result, when the UV laser is tuned to a sharp resonance due to either A or B (as in the case of NATMA), we detect the total fluorescence from both the sharp transition and the broad background. The effect of such contamination of the C5 conformer signals by the C7 “background” can be minimized by operating with low UV laser powers, since the C7 background grows relative to the sharp C5 transitions at higher UV laser power. Even so, the remaining contribution from the broad background must be subtracted out in measuring the total signal due to A or B. These correction factors are typically 10%–12% for the A conformer of NATMA, 10%–15% for the B conformer of NATMA, and 10%–15% for the A conformer of NATA.

As discussed in greater detail in Secs. IV and V, a significant goal of the present work is to obtain conformational isomerization quantum yields for each of the NH stretch fundamentals of all the populated conformers of NATA and NATMA. The determination of such quantum yields rests on two sets of measurements: (i) population transfer spectra for each of the conformations under conditions under which the IR-excited population is completely cooled back down into the zero-point levels prior to UV interrogation [Fig. 6(a)], and (ii) “warm FDIR” spectra for each conformation taken

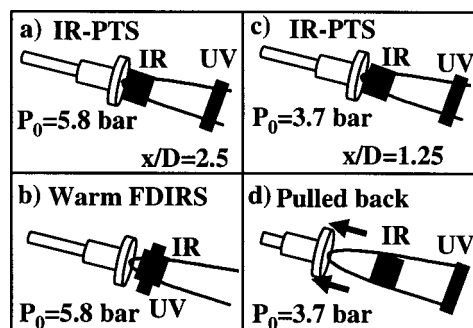


FIG. 6. Schematic diagram of the laser and expansion conditions used in determining isomerization quantum yields. (a) and (b) The method used in this work. Standard supersonic expansion conditions: 5.8 bar backing pressure of helium, and IR excitation 2.5 nozzle diameters ($x/D=2.5$) downstream from the expansion orifice of 800 μm diameter. (a) IR-PTS scans with the UV beam downstream at $x/D=7$ were compared with warm FDIR scans in which the UV overlaps the IR. (c) and (d) Conditions used in the initial report (Ref. 6). Standard supersonic expansion conditions: 3.7 bar backing pressure of helium and infrared excitation at $x/D=1.25$. (d) No-fill conditions were achieved by pulling back the nozzle without moving the IR or UV beams. Under these conditions, the integrated intensity of the IR bands could not be used to establish the fractional population depletion in the absence of hole filling.

under conditions identical to the IR-PTS spectra. Under these conditions, the UV laser is spatially overlapped with the IR beam upstream in the expansion and delayed in time by only 10 ns so that refilling of the IR-excited molecules does not occur [Fig. 6(b)]. The warm FDIR spectra are necessary to assess how much population was excited by the IR laser.

The experimental protocol used in the present work was modified from that used in the initial communication.⁶ In that earlier work, the “no-fill” conditions were achieved simply by pulling back the pulsed valve several nozzle diameters so that IR excitation occurred under conditions where insufficient collisions are present to recoil the molecules [Fig. 6(d)]. These “pulled back” FDIR spectra required no movement of the laser beams, and intensities could be reproduced easily from one scan to the next. However, because IR excitation is occurring in a cooler region of the expansion, the IR bands are narrower than those obtained in the IR population transfer spectra, where the cooling collisions collect population following IR excitation from rotationally warm molecules present upstream. As a result, the shapes of the bands in the population transfer spectra could not be deduced from the pulled back FDIR spectra, requiring independent fitting of the band shapes in the IR population transfer spectra. This is difficult to do in regions where IR bands partially overlap one another. Furthermore, careful analysis of the integrated intensities of the bands in the pulled back FDIR spectra over a wide variety of conditions led to the conclusion that they systematically underestimated the integrated depletion intensities of the bands, and thus skewed the measurements of the “refill” quantum yields. The warm FDIR spectra were recorded with the IR in an identical position to that used for IR-PTS, and thus faithfully reproduced the shape of the bands in the IR-PTS while reflecting the proper no-fill depletion intensity.

The faithful reproduction of shape and intensity of the bands achieved by the warm FDIR spectra was not without

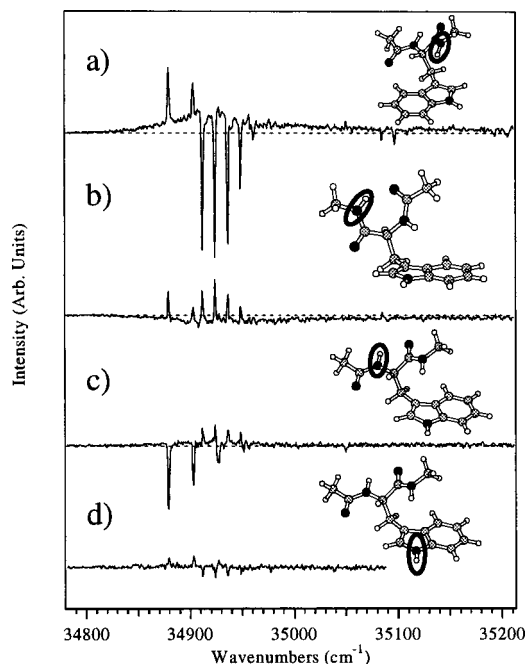


FIG. 7. A series of IR-UV hole-filling spectra recorded with the IR laser fixed on (a) the ψ -amide NH stretch fundamental of conformer B at 3454 cm^{-1} , (b) the H-bonded ψ -amide NH stretch of conformer C at 3340 cm^{-1} , (c) the ϕ -amide NH stretch of conformer A at 3440 cm^{-1} , and (d) the indole NH stretch fundamental of all three conformers at 3523 cm^{-1} . Note that in all cases, the depletion in population in one conformer leads to an increase in population in the other conformers that had a population in them in the absence of the IR.

its price. The warmer conditions encountered by the UV laser when it was upstream in the expansion led to broader LIF bands with a greater potential for contamination of one conformer signal by another. As a result, the position of IR excitation was chosen to achieve greater cooling prior to IR excitation ($x/D=2.5$ compared to $x/D=1.25$ earlier), counteracted by a greater backing pressure ($P_0=5.8$ bar compared to 3.7 bar) to retrieve some of the loss in collision rates so induced.

IV. RESULTS

Figure 7 presents a series of IR-UV hole-filling spectra for NATMA. A comparison of the hole-filling spectrum [Fig. 7(a)] with the LIF spectrum [Fig. 1(a)] leads to an immediate interpretation of the hole-filling spectrum. IR excitation of the 3454 cm^{-1} band of conformer B partially depletes its population, thereby producing dips in the vibronic transitions due to B. This loss in population in conformer B produces gains in population in A (the sharp transitions just to the red of the transitions due to B) and C (the broad background). Similarly, IR excitation of the hydrogen-bonded NH stretch of conformer C [Fig. 7(b)] partially depletes its population, and produces gains in the populations of both A and B. Exciting a transition in conformer A [Fig. 7(c)] drives the population out of that conformer into B and C. Finally, Fig. 7(d) presents a hole-filling spectrum following nonselective excitation of the indole NH stretch fundamental at 3523 cm^{-1} .

Several important deductions can be drawn from this data: First, the spectra clearly demonstrate the feasibility of

using IR excitation to selectively excite a single conformation in a mixture of conformational isomers. Second, this selective excitation effectively creates a conformational population distributions downstream in the expansion, and moves the experimentalist beyond simply “taking what nature provides” in the supersonic expansion process. Third, selective IR excitation redistributes the population between the same three conformers that had a population in them in the absence of IR excitation; that is, no additional isomers are observed downstream. One of the hopes for the method was that the selective excitation and fast cooling might trap a population in conformational minima that did not have a significant population in the absence of the IR excitation. However, in neither NATMA nor NATA was this observed. Fourth, the process is quite efficient. At the highest IR powers, it is possible to deplete a large fraction of the ground-state population of a given conformer. This can produce substantial changes in the population downstream. Finally, the small population transfer induced by the nonselective excitation of the indole NH stretch fundamental makes it clear that large population changes require selective excitation. When all three conformers absorb the same amount of energy with equal efficiency, little net change in population is observed.

Figures 8 and 9 display a series of population transfer spectra and upstream FDIR spectra for NATMA and NATA, respectively, taken under the “standard” conditions depicted in Figs. 6(a) and 6(b). The traces in Figs. 8 and 9 are weighted sums of three independent data sets. These data sets are used to extract isomerization quantum yields for each of the six independent NH stretch transitions of NATMA (three conformers with two amide NH stretch fundamentals each) and NATA (two conformers with three amide NH stretch modes each). We now turn our attention to the methods used to analyze the data and extract isomerization quantum yields.

V. ANALYSIS

A. The fundamental equations

A population transfer spectrum monitoring conformer “A” measures the fractional change in the population *downstream* following: (i) IR excitation *upstream* and (ii) *recooling* in the expansion as the molecules traverse from the excitation to the detection volumes. Consider an IR frequency $\tilde{\nu}$ at which all three isomers have an IR absorption. At that frequency, the change in number density of a given conformer (e.g., A) downstream in the expansion, $\Delta N_A^{dn}(\tilde{\nu})$, is given by

$$\Delta N_A^{dn}(\tilde{\nu}) = \Delta N_A^{up}(\tilde{\nu}) \cdot (1 - \Phi_{AA}(i)) \cdot \left(\frac{N_A^{dn}}{N_A^{up}} \right) \cdot \phi_A^* - \sum_{I=B,C} \Delta N_I^{up}(\tilde{\nu}) \cdot \Phi_{IA}(j) \cdot \left(\frac{N_I^{dn}}{N_I^{up}} \right) \cdot \phi_I^*, \quad (1)$$

where $\Delta N_I^{up}(\tilde{\nu})$ is the number density of *I* excited upstream, $[1 - \Phi_{AA}(i)]$ is the fraction of excited A molecules that isomerize out of A due to IR transition “*i*,” $\Phi_{IA}(j)$ is the fraction of conformer I excited via infrared transition “*j*”

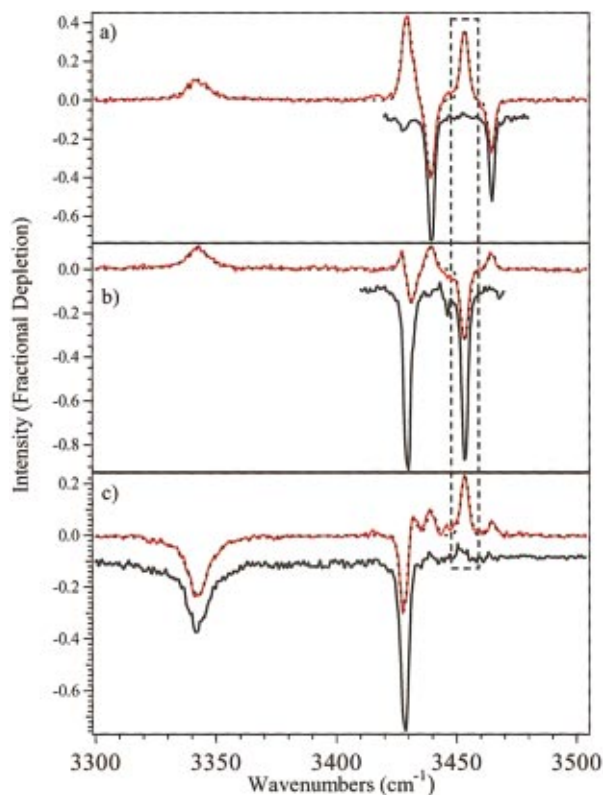


FIG. 8. (Color) IR-population transfer spectra (red trace above) and upstream FDIR spectra (black trace below) monitoring the population in (a) conformer A via its S_0-S_1 origin at $34\,880\text{ cm}^{-1}$, (b) conformer B via its S_0-S_1 vibronic band at $34\,925\text{ cm}^{-1}$, and (c) conformer C via its absorption at $34\,968\text{ cm}^{-1}$. The black dashed lines overlaid with the IR population transfer spectra represent the calculated fit that was used to extract quantitative information. The upstream FDIR scans determine the fractional population of each conformer excited by the infrared, while the PT spectra measure the fractional change in population of each conformer. The transitions enclosed in the black rectangle show the contributions needed to determine the isomerization quantum yields Φ_{BA} , Φ_{BB} , and Φ_{BC} for the 3454 cm^{-1} band of conformer B.

that isomerizes into A, $N_1^{\text{dn}}/N_1^{\text{up}}$, is the fractional change in number density of conformer I during expansion from upstream to downstream, and ϕ_1^* is the transport efficiency of the excited molecules by comparison to the unexcited molecules. The quantities $\Phi_{IJ}(i)$ are quantum yields for isomerizing I to J following excitation of infrared transition i , and are the quantities we seek to measure. The transport efficiency ϕ_1^* would be less than 1.0 if the IR-excited molecules were transported in the jet differently than those which are not IR excited (by virtue of the extra energy they receive from IR excitation). We have measured this transport efficiency in 5-methoxy NATMA, a close analog of NATMA that possesses only a single conformational isomer. Since the hole-filling signal for this molecule was zero (i.e., the hole created by the IR laser was filled in completely), the transport efficiency of A^* equals that of A. Therefore, in what follows, we have set $\phi_1^* = 1$ for all conformers.

If we divide through both sides of Eq. (1) by N_A^{dn} , and recognizing that the ratio of downstream populations ($N_1^{\text{dn}}/N_A^{\text{dn}}$) equals the ratio of fractional populations,

$$N_1^{\text{dn}}/N_A^{\text{dn}} = (N_1^{\text{dn}}/N_{\text{tot}}^{\text{dn}})/(N_A^{\text{dn}}/N_{\text{tot}}^{\text{dn}}) = (F_1^{\text{dn}}/F_A^{\text{dn}}),$$

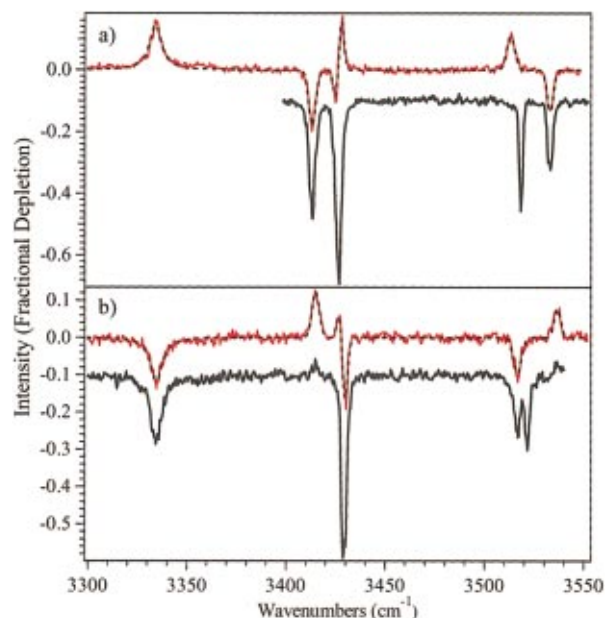


FIG. 9. (Color) Analogous scans to those in Fig. 8 for NATA. Conformer A and B of NATA are assigned to the same conformations as B and C of NATMA.

Eq. (1) becomes

$$\frac{\Delta N_A^{\text{dn}}(\tilde{\nu})}{N_A^{\text{dn}}} = \frac{\Delta N_A^{\text{up}}(\tilde{\nu})}{N_A^{\text{up}}} \cdot (1 - \Phi_{AA}(i)) - \frac{\Delta N_B^{\text{up}}(\tilde{\nu})}{N_B^{\text{up}}} \cdot \Phi_{BA}(j) \cdot \left(\frac{F_B^{\text{dn}}}{F_A^{\text{dn}}} \right) - \frac{\Delta N_C^{\text{up}}(\tilde{\nu})}{N_C^{\text{up}}} \cdot \Phi_{CA}(k) \cdot \left(\frac{F_C^{\text{dn}}}{F_A^{\text{dn}}} \right). \quad (2)$$

The fractional change in the downstream population of each conformer is determined by recording a population transfer spectrum for each conformer. Similarly, the fractional population that absorbs an IR photon is measured by a FDIR spectrum recorded with the UV moved upstream to overlap the IR beam in the collision-dominated region of the expansion, with a 10 ns delay time between the IR and the UV lasers. Under these conditions, no refilling of the population has occurred, and only dips appear in the spectrum. By recording the upstream FDIR spectra under identical conditions to the population transfer spectra, quantitative comparison can be made. Both types of spectra are recorded in active baseline subtraction mode in which the difference in fluorescence signal with and without the IR laser is recorded. By taking the ratio of this differential signal to the absolute fluorescence signal in the absence of the IR, a fractional population change, $\Delta N_1/N_1$, is recorded for each conformer. The absolute scales on these spectra are affected by the degree of overlap of the LIF laser with the IR-excited molecules:

$$\frac{\Delta N_A^{\text{dn}}(\tilde{\nu})}{N_A^{\text{dn}}} = \frac{I_A^{\text{PT}}(\tilde{\nu})}{\phi_{\text{over}}^{\text{dn}}} \quad \text{and} \quad \frac{\Delta N_1^{\text{up}}(\tilde{\nu})}{N_1^{\text{up}}} = \frac{I_A^{\text{FDIR,up}}(\tilde{\nu})}{\phi_{\text{over}}^{\text{up}}}. \quad (3)$$

This leads to a final set of equations applicable to the general case in which all three conformers have an absorption that contributes to the spectrum at a particular wave number $\tilde{\nu}$:

$$I_A^{PT}(\tilde{\nu}) = \left[I_A^{FDIR,up}(\tilde{\nu}) \cdot (1 - \Phi_{AA}(i)) - I_B^{FDIR,up}(\tilde{\nu}) \cdot \left(\frac{F_B^{dn}}{F_A^{dn}} \right) \cdot \Phi_{BA}(j) - I_C^{FDIR,up}(\tilde{\nu}) \cdot \left(\frac{F_C^{dn}}{F_A^{dn}} \right) \cdot \Phi_{CA}(k) \right] \cdot \gamma,$$

$$I_B^{PT}(\tilde{\nu}) = \left[- \left(\frac{F_A^{dn}}{F_B^{dn}} \right) I_A^{FDIR,up}(\tilde{\nu}) \cdot \Phi_{AB}(i) + I_B^{FDIR,up}(\tilde{\nu}) \cdot (1 - \Phi_{BB}(j)) - I_C^{FDIR,up}(\tilde{\nu}) \cdot \left(\frac{F_C^{dn}}{F_B^{dn}} \right) \cdot \Phi_{CB}(k) \right] \cdot \gamma,$$

$$I_C^{PT}(\tilde{\nu}) = \left[- \left(\frac{F_A^{dn}}{F_C^{dn}} \right) I_A^{FDIR,up}(\tilde{\nu}) \cdot \Phi_{AC}(i) - I_B^{FDIR,up}(\tilde{\nu}) \cdot \left(\frac{F_B^{dn}}{F_C^{dn}} \right) \cdot \Phi_{BC}(j) + I_C^{FDIR,up}(\tilde{\nu}) \cdot (1 - \Phi_{CC}(k)) \right] \cdot \gamma,$$
(4)

where $\gamma = (\phi_{over}^{dn} / \phi_{over}^{up})$. Note that the term $(1 - \Phi_{JJ})$ gives the quantum yield for leaving conformation J, and produces a dip in the population transfer spectrum, while the other two terms are gains in population of J, and therefore appear with opposite sign. By choosing conditions in which the infrared laser beam is two to three times larger than the UV beam, the UV probe laser intersects the central portion of this excitation volume. Scans of the timing between the two lasers map out the relative sizes of the beams as the excited molecules move past the probe beam due to the velocity of the expansion. Since the excitation volume expands in size as the free jet expands, the probe beam intersects the central portion of the excitation volume in either case, so that maximizing the gains and dips in the spectrum sets laser timing in which the overlap is complete in both upstream and downstream configurations. As a result, $\gamma = 1$.

In summary, in order to determine isomerization quantum yields, it is necessary to measure a set of population transfer spectra, $I_J^{PT}(\tilde{\nu})$ for each of the conformers, a corresponding set of "upstream" FDIR spectra for these conformers, $I_J^{FDIR,up}(\tilde{\nu})$, and their fractional populations, F_J^{dn} , in the absence of infrared excitation.

B. Determining the fractional conformational populations in the absence of infrared excitation

Figure 10(a) presents an overlay of the population transfer spectra monitoring conformers A–C of NATMA. It is obvious from this overlay that there is a reflection symmetry to these spectra, in which depletions in one spectrum are always compensated for by gains in other spectra. Since the hole-filling spectra did not detect the formation of any conformational minima produced by infrared excitation, then as long as recooling is complete, there is no net change in the population of the three conformations; that is, at all infrared frequencies,

$$\Delta N_{tot}^{dn}(\tilde{\nu}) = \Delta N_A^{dn}(\tilde{\nu}) + \Delta N_B^{dn}(\tilde{\nu}) + \Delta N_C^{dn}(\tilde{\nu}) = 0. \quad (5)$$

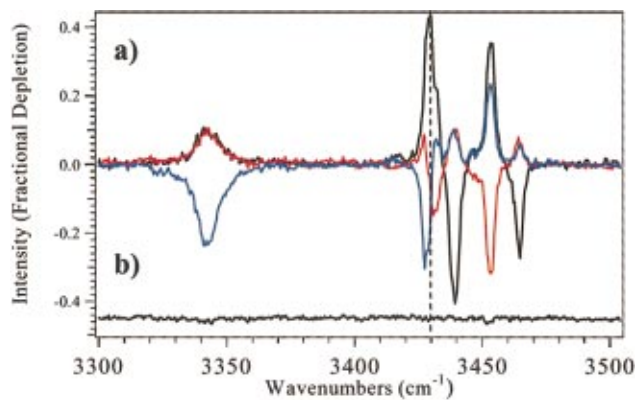


FIG. 10. (Color) (a) An overlay of the population transfer spectra of NATMA conformers A (black), B (red), and C (blue) showing the reflection symmetry of the population transfer spectra. By proper choice of IR wavelength, it is possible to change the downstream conformational population distribution, increasing one or more populations at the expense of the others. (b) Weighted sum of the population transfer spectra, $F_A I_A^{PT} + F_B I_B^{PT} + F_C I_C^{PT}$, that goes to zero at all IR wavelengths. The weighting factors F_I are the fractional populations of conformers A, B, and C in the expansion in the absence of the IR radiation.

Substituting for ΔN_I^{dn} from Eq. (3) yields a constraining equation for the weighted sum of population transfer spectra at all IR wavelengths,

$$F_A^{dn} \cdot I_A^{PT}(\tilde{\nu}) + F_B^{dn} \cdot I_B^{PT}(\tilde{\nu}) + F_C^{dn} \cdot I_C^{PT}(\tilde{\nu}) = 0. \quad (6)$$

Satisfaction of Eq. (6) over the entire wavelength range of the population transfer spectra constitutes a stringent test that all the IR excited population is accounted for by a redistribution of population among the three detected conformers. In fact, it can easily be shown by substituting Eq. (4) into Eq. (6) that requiring that Eq. (6) be satisfied for a given IR band is equivalent to assuming that the sum of the isomerization quantum yields for that band equals one; that is, for absorption i of conformer A,

$$\Phi_{AA}(i) + \Phi_{AB}(i) + \Phi_{AC}(i) = 1. \quad (7)$$

Figure 10(b) presents a weighted sum of population transfer spectra for NATMA calculated with $F_A^{dn} = 0.20$, $F_B^{dn} = 0.50$, and $F_C^{dn} = 0.30$ under the conditions of our experiment. With this choice of fractional populations, Eq. (6) is satisfied over the entire 3300–3600 cm^{-1} region of interest here. One sigma error bars on these fractional populations are ± 0.02 . Note that these fractional populations neither depend on the value of γ , nor on the upstream FDIR spectra, $I_J^{FDIR,up}$. The analogous data for the two conformers of NATA (not shown) are $F_A^{dn} = 0.44$ and $F_B^{dn} = 0.56$.

Equation (6) provides a quite general method for determining the fractional populations of the conformations of flexible molecules in the supersonic expansion, accurate to within a few percent. Note that this measurement does not depend on the fluorescence quantum yields, electronic oscillator strengths, or Franck–Condon factors of vibronic transitions in the LIF spectra of the conformers, as would be the case if the relative intensities of transitions in the LIF spectra were used to extract relative populations.

C. Method for extracting isomerization quantum yields

The series of population transfer spectra shown in Fig. 8 provides the raw data needed to extract the six sets of isomerization quantum yields for the six unique amide NH stretch IR fundamentals of NATMA (two per conformer, three conformers). The analogous spectra for NATA are shown in Fig. 9. The population transfer spectra have overlaid on them linear-least-squares fits to the data. The isomerization quantum yields are fairly insensitive to the precise form of the fitting function used. All of the bands except the H-bonded NH stretch of conformer C were fit well by Gaussians with widths $\sigma_j(i)$ of 2.0–2.5 cm^{-1} :

$$I_j^{\text{PT}}(\tilde{\nu}) = \frac{I_j^{\text{PT,int}}(i)}{\sqrt{2\pi} \cdot \sigma_j(i)} \cdot \exp\left[-\frac{(\tilde{\nu} - \tilde{\nu}_0(i))^2}{2\sigma_j(i)^2}\right]. \quad (8)$$

The H-bonded NH stretch fundamental, is unusually broad with more pronounced wings that were better fit by a Lorentzian fitting function. The upstream FDIR spectra are used to set the center frequencies and constrain the widths of the IR bands in the fits of the population transfer spectra. The population transfer and upstream FDIR spectra mimic each other so closely because the two are taken under identical conditions of IR excitation. Independent knowledge of the shape of the bands is particularly important for regions of the population transfer spectra where IR bands are partially overlapped.

In some data sets, a small but systematic difference was noted between the band shapes present in the population transfer and upstream FDIR spectra. In these cases, the population transfer spectra were slightly broader (by about 0.5 cm^{-1}) than their upstream FDIR counterparts. This difference has a simple physical interpretation. The population transfer spectra monitor the population changes induced *downstream* by infrared excitation upstream. High rotational levels present upstream are responsible for wings in the IR spectra that contribute to the population transfer signal. However, in the upstream FDIR spectra, the UV laser monitors the peak of the transition in the LIF spectrum, which is dominated by low J rotational levels. As a result, the high J population contributes less to the upstream FDIR spectra (with no cooling present) than the population transfer spectra, leading to slightly broader bands in the population transfer spectra than in the upstream FDIR spectra. As a result, in extracting isomerization quantum yields, we used the fitted peak intensities rather than the integrated peak intensities in order to minimize this difference between the two spectra.

The fitted peak intensities of the bands in the population transfer spectra are then used in conjunction with the fitted peak intensities of the upstream FDIR spectra to obtain the quantum yields. For example, for an NH stretch fundamental of conformer A, we have

$$I_A^{\text{PT,pk}}(i) = I_A^{\text{FDIR,pk}}(i) \cdot (1 - \Phi_{\text{AA}}(i)), \quad (9a)$$

$$I_B^{\text{PT,pk}}(i) = -\left(\frac{F_A^{\text{dn}}}{F_B^{\text{dn}}}\right) \cdot I_A^{\text{FDIR,pk}}(i) \cdot \Phi_{\text{AB}}(i), \quad (9b)$$

$$I_C^{\text{PT,pk}}(i) = -\left(\frac{F_A^{\text{dn}}}{F_C^{\text{dn}}}\right) \cdot I_A^{\text{FDIR,pk}}(i) \cdot \Phi_{\text{AC}}(i). \quad (9c)$$

The analogous equations for absorption ‘‘j’’ of conformer ‘‘B’’ are

$$I_A^{\text{PT,pk}}(j) = -I_B^{\text{FDIR,pk}}(j) \cdot \left(\frac{F_B^{\text{dn}}}{F_A^{\text{dn}}}\right) \cdot \Phi_{\text{BA}}(j), \quad (10a)$$

$$I_B^{\text{PT,pk}}(j) = I_B^{\text{FDIR,pk}}(j) \cdot (1 - \Phi_{\text{BB}}(j)), \quad (10b)$$

$$I_C^{\text{PT,pk}}(j) = -I_B^{\text{FDIR,pk}}(j) \cdot \left(\frac{F_B^{\text{dn}}}{F_C^{\text{dn}}}\right) \cdot \Phi_{\text{BC}}(j). \quad (10c)$$

Finally, absorption ‘‘k’’ of conformer ‘‘C’’ is governed by

$$I_A^{\text{PT,int}}(k) = -I_C^{\text{FDIR,pk}}(k) \cdot \left(\frac{F_C^{\text{dn}}}{F_A^{\text{dn}}}\right) \cdot \Phi_{\text{CA}}(k), \quad (11a)$$

$$I_B^{\text{PT,int}}(k) = -I_C^{\text{FDIR,pk}}(k) \cdot \left(\frac{F_C^{\text{dn}}}{F_B^{\text{dn}}}\right) \cdot \Phi_{\text{CB}}(k), \quad (11b)$$

$$I_C^{\text{PT,pk}}(k) = I_C^{\text{FDIR,pk}}(k) \cdot (1 - \Phi_{\text{CC}}(k)). \quad (11c)$$

Since the peak intensities of the population transfer and upstream FDIR spectra are measured experimentally, and the weighted sums of population transfer spectra provide the downstream fractional populations $\{F_i^{\text{dn}}\}$, the only unknowns are the desired quantum yields Φ_{ij} . For example, for the *i*th NH stretch fundamental of conformer A, the only unknown in Eq. (9a) is $\Phi_{\text{AA}}(i)$. Similarly Eqs. (9b) and (9c) determine $\Phi_{\text{AB}}(i)$ and $\Phi_{\text{AC}}(i)$, respectively. By treating the three quantum yields as independently measured quantities, one can check whether they add to 1.0 as they should, i.e., $\Phi_{\text{AA}}(i) + \Phi_{\text{AB}}(i) + \Phi_{\text{AC}}(i) = 1$. This is typically satisfied to within the error of the measurement, but when it is not, it often signals the presence of a systematic error in the data set. It thereby played a crucial role in refining the experimental method.

Error analysis is carried out using the sum of the χ^2 for the best fits to each population transfer spectrum, $\chi_{\text{min,tot}}^2$ to establish a $\chi_{\text{max,tot}}^2$ consistent with a one-standard deviation error.⁹ By stepping along three constant-yield lines from the center point, errors on the band intensities are obtained when χ_{max}^2 is exceeded. By propagating the errors on these intensities through the quantum yield formulas of Eqs. (9)–(11), including the error on the warm FDIRS spectrum, errors on the quantum yields are obtained.

Contributions to the error in the quantum yields due to noise in the population transfer and upstream FDIR scans, the fractional population measurement, background correction, long-term drift in the probe signal, and the peak widths and positions used in the fitting were tested. Of these, the dominant contributions to the error arose from the noise in the population transfer and upstream FDIR scans, which contributed about equally to the final error. In addition, the isomerization quantum yields were found to be sensitive to the center frequency of the IR transitions used in the fitting routine (especially in regions of overlapping peaks). How-

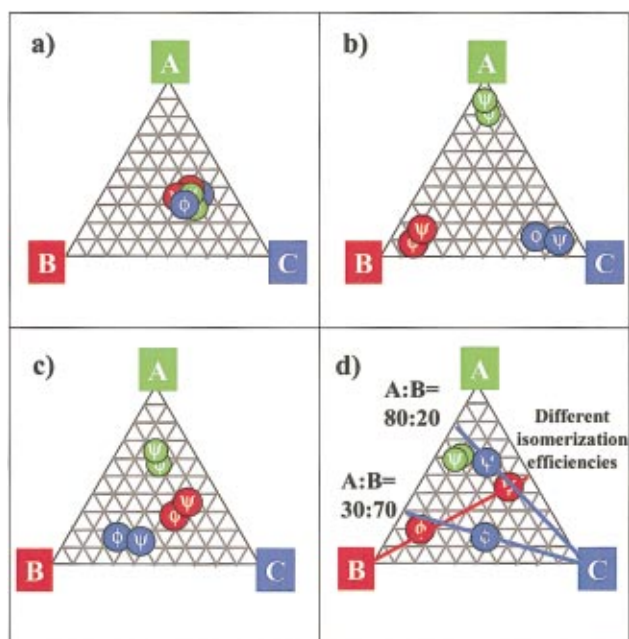


FIG. 11. (Color) Schematic triangular plots of the product quantum yields demonstrating the appearance of the plots under various limiting cases for the isomerization process. A single point on the triangle plot locates a set of three quantum yields for a given IR band of a particular conformer. The size of the circle indicates the error associated with the measurement. (a) The result if isomerization is fast compared to cooling, so that equilibrium product yields are established. (b) The result if cooling were fast compared to isomerization, with little net reaction occurring. (c) A set of conformer specific quantum yields. (d) Quantum yields that are both conformer specific and vibrationally mode specific. The ϕ - and ψ -amide NH stretch modes of C are here shown to have different product quantum yields (blue lines). The analogous bands of conformer B are shown to have similar product yields, but differing isomerization efficiencies, Φ_{BB} .

ever, in all cases, the upstream FDIR value was used for the center frequency, since in the transitions where there was no overlap, the peak frequencies of the upstream FDIR and population transfer spectra were equal.

D. Displaying the quantum yield results: Triangular plots

The isomerization quantum yields for NATMA specify the fractional abundances of the three conformers A, B, and C following excitation of a single conformation in one of the amide NH stretches (labeled as ϕ or ψ depending on whether the ϕ -amide or ψ -amide NH stretch is excited). We have found it useful to plot each set of isomerization quantum yields as a point on a triangular plot similar in appearance to a three-component phase diagram, as shown in schematic form in Fig. 11. Each set of best-fit quantum yields constitutes a single point on the diagram, with one-sigma errors in Φ_{XA} , Φ_{XB} , and Φ_{XC} producing irregular shapes about this central point.

A particular advantage of summarizing the data in this way is that various limiting cases for the results are easily depicted and identified. As Fig. 11(a) shows, if cooling occurs on a time scale much slower than isomerization, then an equilibrium product distribution will be achieved which is independent of which conformation is excited and in which vibrational mode. In the other extreme, when cooling occurs

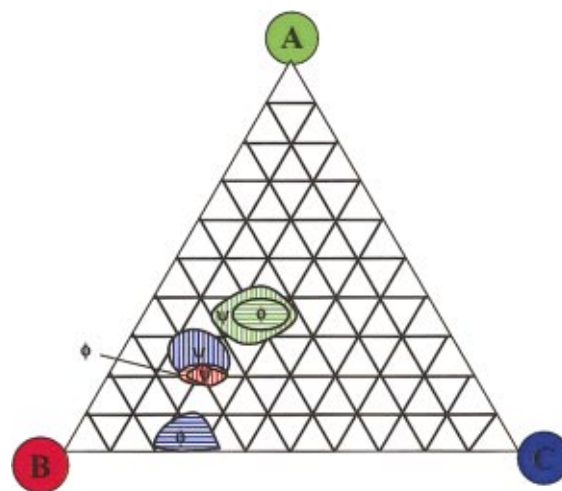


FIG. 12. (Color) Experimental isomerization quantum yields for NATMA. The fractional populations downstream in the expansion without the IR present are $F_A=0.20$, $F_B=0.50$, and $F_C=0.30$ for NATMA.

quickly compared to the rate of isomerization out of the initial conformational well, then most of the excited population will be stabilized in the initial well, leading to a quantum yield diagram like that in Fig. 11(b). Of course, it is possible that such a limiting case could never be achieved if the states accessed by the initial vibrational excitation are inherently conformationally mixed.

From the standpoint of chemical dynamics, the cases portrayed in Figs. 11(c) and 11(d) are much more interesting. Figure 11(c) portrays a case where the isomerization is *conformation specific* but not *mode specific*. In this case, the product quantum yields vary from one conformation to the next, but are independent of which vibrational mode is initially excited within a given conformation. The highest degree of selectivity is depicted in Fig. 11(d), where both conformation and mode specificity is achieved. There are two ways in which this mode-specificity could appear. As shown in Fig. 11(d) for the quantum yields associated with excitation of conformer B, vibrational mode specificity could lead to different yields of the two conformational products (e.g., 70:30 or 20:80 in the diagram). Alternatively, the mode specificity could appear as differences in the isomerization efficiency without substantially changing the yields of the products (as shown for the ϕ - and ψ -amide NH stretches of A).

E. Isomerization quantum yields for N-acetyl tryptophan methyl amide and N-acetyl tryptophan amide

The triangular plot in Fig. 12(a) summarizes the six sets of experimentally determined isomerization quantum yields for NATMA. Also included in the plot is the fractional conformational population distribution in the absence of the IR radiation, determined by zeroing the weighted sum of the population transfer spectra, as described in Sec. IV B. The results are also summarized in Tables I and II to ensure quantitative accuracy. The analogous data for the two-conformation case of NATA, are given in Table II. The error

TABLE I. IR-induced isomerization quantum yields and fractional populations of the conformational isomers in the absence of infrared radiation for NATMA.

Quantum yields ^b	Fractional population ^c	Isomerization quantum yields for NATMA ^a					
		NATMA A		NATMA B		NATMA C	
		3440 cm ⁻¹	3466 cm ⁻¹	3431 cm ⁻¹	3454 cm ⁻¹	3340 cm ⁻¹	3429 cm ⁻¹
Φ_{XA}	0.20±0.02	0.38±0.04	0.38±0.07	0.20±0.03	0.20±0.03	0.25±0.07	0.06 ± $\frac{0.05}{0.03}$
Φ_{XB}	0.50±0.02	0.37±0.06	0.39±0.09	0.59±0.04	0.60±0.03	0.57±0.07	0.77 ± $\frac{0.06}{0.08}$
Φ_{XC}	0.30±0.02	0.24±0.06	0.22±0.08	0.21±0.04	0.19±0.04	0.18±0.08	0.18 ± $\frac{0.06}{0.05}$

^aQuantum yields have been normalized so that their sum equals 1.0. Errors represent one standard deviation.

^bFirst subscript represents the initial population (i.e., A, B, or C), second subscript represents final population.

^cPopulation in the expansion in the absence of IR laser.

bars on these data (NATA) are somewhat larger due to the lower overall signal of NATA versus NATMA.

By necessity, the methods used to determine isomerization quantum yields involve IR-exciting and isomerizing substantial fractions of the populations of the conformational minima. In order to assess the extent and effect of multiphoton IR absorption on the isomerization quantum yields, population transfer spectra and isomerization quantum yields were determined for NATMA over a range of IR powers. These were determined by two independent methods. In the first method, the effect of IR power on the ν -amide NH stretching mode of conformer B was studied. A series of IR neutral density filters were used to attenuate the 1.5 mJ/pulse IR beam by up to a factor of 4. Population transfer quantum yields were determined with the IR laser wavelength fixed at the peak of the infrared transition. This technique allowed us to record intensity changes simply by adding or removing neutral density filters. In addition, a full set of population transfer and warm FDIR spectra were recorded for three of the most intense bands in the IR with the IR laser power attenuated by a factor of 4. In all cases, the derived quantum yields were found to lie within one standard deviation of the results listed in Tables I and II.

VI. DISCUSSION

The experimental methods of IR-UV HFS and IR-PTS probe the dynamics of conformational isomerization using a unique cool-pump-cool-probe configuration that provides for conformation-specific excitation and detection sandwiched between a fast cooling step in the early portions of a supersonic free jet. The method is capable of inducing significant laser-controlled changes in the conformational population downstream in the expansion. By proper choice of IR wavelength, population can be driven out of a single conformation of choice, leading to population gains in other conformations. While the population changes induced in the present experiment are rather modest, it is worth speculating briefly on what could be possible. Ideally, one would hope to achieve a downstream population that is nearly pure in a user-controlled conformation. Clearly, this cannot be achieved completely by excitation at a single IR wavelength. However, there are particular wavelengths where partial

overlap of two or more bands can lead to a maximization of a particular product. For instance, IR excitation at 3430 cm⁻¹ in NATMA [indicated by a dotted line in Fig. 10(b)] partially depletes the populations of both C and B, thereby producing a “double gain” in A that will maximize its downstream population relative to the others. One could imagine more complicated scenarios in which a high-power broadband IR beam is configured with an intensity pattern designed to maximize the production of a particular product at the expense of all others. In principle, the makeup of this wavelength-controlled laser pulse (even without the phase control associated with a coherent control experiment) could be predicted from the individual IR population transfer spectra, or searched for in an automated feedback loop.

The primary quantitative results of this work are (i) fractional conformational populations of NATMA and NATA in the absence of IR excitation, and (ii) isomerization quantum yields following selective IR excitation of single conformations in well-defined NH stretch modes.

A. Comparing the fractional populations of N-acetyl tryptophan methyl amide and N-acetyl tryptophan amide

The fractional populations of NATMA and NATA are summarized in Tables I and II. It is striking that the number of conformational isomers with significant population changes from NATMA to NATA, given their close structural similarity. It is the C5(AΦ) conformer that is missing in NATA. This conformer has the smallest population of the three observed in NATMA, and does tend to be somewhat smaller in fractional population under more severe cooling conditions. The complete removal of C5(AΦ) population in NATA could signify either a reduction in the population prior to expansion or a more efficient collisional removal of this population during expansion.

In retrospect, this dependence of the fractional populations on the expansion conditions and precise chemical structure is not too surprising, given the sensitivity of the conformer energies to weak interactions between parts of the molecule, combined with the complicated kinetics of conformational cooling in the expansion. The fractional populations for NATMA listed in Table I are for a backing pressure of 5.8 bar helium and an 800 μm diameter expansion orifice, and

TABLE II. IR-induced isomerization quantum yields and fractional populations of the conformational isomers in the absence of IR radiation for NATA.

Quantum yields ^b	Fractional population ^c	Isomerization quantum yields for NATA ^a					
		NATA A			NATA B		
		3417 cm ⁻¹	3428 cm ⁻¹	3538 cm ⁻¹	3334 cm ⁻¹	3429 cm ⁻¹	3516 cm ⁻¹
Φ_{XA}	0.44±0.03	0.53±0.09	0.49±0.10	0.47±0.07	0.64±0.05	0.66±0.11	0.64±0.12
Φ_{XB}	0.56±0.03	0.47±0.09	0.51±0.10	0.53±0.07	0.36±0.05	0.34±0.11	0.36±0.12

^aQuantum yields have been normalized so that their sum equals 1.0. Errors represent one standard deviation.

^bFirst subscript represents the initial population (i.e., A or B), second subscript represents final population.

^cPopulation in the expansion in the absence of IR laser.

differ somewhat from that reported earlier⁶ under somewhat less severe expansion conditions ($F_A=0.23$, $F_B=0.40$, and $F_C=0.37$). A comparison of the fractional populations of NATMA and NATA suggests that the population in C5(A Φ) in NATMA is collected into the C7(Φ P) conformer in NATA. However, it is not obvious from the disconnectivity diagram of NATMA [Fig. 2 of the adjoining paper (Ref. 10)] that such a selective cooling route exists, and other explanations may be responsible for the disappearance of the C5(A Φ) conformer in NATA.

B. Evaluation of the isomerization quantum yields

Several deductions follow immediately from the isomerization quantum yields summarized in Fig. 12: First, the product quantum yields generally fall in the same region of the diagram as the population distribution in the absence of the IR; that is, conformations with a large population in the absence of infrared typically receive a substantial fraction of the IR-excited population as well. Second, the spread in quantum yields over the six vibrational fundamentals is rather modest, indicating that the populations are approaching equilibrium during the cooling process [Fig. 11(a)]. Third, there is some degree of conformational specificity to the product quantum yields, both in NATMA and NATA. For example, the quantum yields following the excitation of NATMA(A) lie nearly coincident with one another, but distinct from the pair of results associated with excitation of NATMA(B). Similarly, the three NH stretch modes of NATA(B) are shifted from those due to NATA(A), showing a slight preference for excited A conformers to form B and vice versa. The fact that IR pumping of one isomer preferentially forms the other isomer suggests that multiphoton effects may contribute to the observed quantum yields in NATA.

Finally, there are hints of vibrational mode selectivity in the quantum yields, though less striking than in the earlier report.⁶ For instance, the two amide NH stretch fundamentals of conformer C of NATMA exhibit differences in their quantum yields that lie just outside the error bars separating them. This C7_{eq} conformation has a unique dipeptide backbone that directly involves the ψ -amide NH group in an H bond, and thereby holds the ϕ -amide NH group in a unique configuration as well. This could predispose this conformer to mode-specific effects involving the dynamics of breaking this hydrogen bond during the isomerization process.

C. Infrared-induced conformational isomerization in flexible biomolecules

A detailed analysis of the isomerization pathways, time scales, and collisional cooling rates in NATMA is given in the adjoining paper (Ref. 10). Here, we present a more general discussion of IR-induced conformational isomerization in flexible molecules of this size and the prospects for seeing more dramatic conformation specific and vibrationally mode specific effects in experiments of this type.

Based on a calculation using harmonic frequencies for a single conformer, we estimate that the conformational isomers of NATMA and NATA possess an average vibrational energy of about 7000 cm⁻¹ prior to expansion. This energy is collisionally removed to produce an initial conformational population distribution largely in its zero-point levels, and then reexcited with about half of this energy (~ 3500 cm⁻¹) by absorption of an IR photon. The excited molecules undergo a similar collisional cooling, but starting from the unique conditions associated with excitation of a single conformation in a well-defined NH stretch oscillator. The isomerization process thus contains both intramolecular dynamics associated with coupling the localized vibrational excitation into the other vibrational states of the molecule, and collisional effects, which can accomplish the same thing as they cool the molecule. The hole-filling experiment only probes the end result of both these processes. As a result, it is difficult to sort out the contributions from each to the observed isomerization quantum yields. Furthermore, given the fact that the experiment lacks a direct probe of the events that link initial excitation to final product, a full state-to-state description of the process would seem challenging, hopeless, or irrelevant, depending on one's viewpoint regarding the prospects for mode specific effects in molecules of this size and conformational complexity.

It is clear how to proceed if one ignores the possibility of such mode specific effects. In this case, one can consider the experiment as a kinetic process that begins from a single conformation with a well-defined internal energy, and proceeds as a series of isomerization steps involving passage over transition states separating connected minima. Such theoretical modeling necessarily must address the inherent complexity of the potential energy surface, in which multiple competing pathways exist between any two conformational minima. However, calculation of the microcanonical rate constant $k(E)$ for any one step is the everyday task of RRKM theory, especially if one assumes a harmonic descrip-

tion of the vibrational states of each reactant and transition state. This is the tactic taken in the adjoining paper (Ref. 10). However, Rice–Ramsperger–Kassel–Marcus (RRKM) theory assumes that $k(E)$ is determined solely by the full vibrational state densities of the reactant and transition state, assuming no distinction between one state and another.

The hole-filling experiment is initiated by IR excitation of a single well-defined NH stretch fundamental, and therefore might differ in its dynamics from that coming from a statistical sample of all vibrational states at that energy. The NH($\nu=1$) level accessed by the IR excitation is coupled to this full set of vibrational levels via coupling strengths that vary over an enormous range. This vibrational state mixing, commonly known as intramolecular vibrational redistribution (IVR), is a subject of intense, ongoing study of enormous importance to our understanding of energy flow in molecules.^{11–14} Great progress has been made in both experimental and theoretical studies of IVR.^{11–20} Most of that work has been on nonreacting molecules that have a single minimum or a well-defined set of minima associated with a single large-amplitude coordinate (e.g., the internal rotation of a methyl group).

Among the most relevant of these studies for the present discussion are the recent, elegant microwave-IR double resonance studies of Pate and co-workers.¹³ These spectra probe the rotational structure of individual eigenstates following vibrational excitation of an XH fundamental in a molecule which can undergo hindered internal rotation between two distinct conformational minima (e.g., gauche or anti 1,2-disubstituted ethanes). Since the XH($\nu=1$) level accessed by the IR excitation is above the barrier-to-conformational isomerization, the full vibrational density of states includes levels that are conformationally mixed in character. The microwave spectra of the IR-excited levels reflect a mixing of the XH($\nu=1$) level with this full density of vibrational states, including eigenstates that are primarily localized over the other conformational well, or even over the transition state.

The present experiment probes molecules with more than 30 atoms and several flexible sites that substantially increase its vibrational and conformational complexity.²¹ The size and flexibility of the molecule are already evident in a harmonic description of the vibrations in a single conformational well. There are 102 vibrational degrees of freedom in NATMA, eight of which have harmonic frequencies below 100 cm^{-1} . According to a harmonic vibrational frequency estimate, each conformational well supports a vibrational state density of about 10^{14} vibrational states/ cm^{-1} at an energy 3500 cm^{-1} (10 kcal/mol) above the zero-point level. This staggering number does not take into account the large anharmonic corrections associated with torsional degrees of freedom above the barrier(s) to conformational isomerization. Furthermore, the full density of vibrational states at the energy of the XH($\nu=1$) level of a single conformational isomer includes contributions from some 60 conformational minima connected by multiple pathways, many of which involve large geometry changes.

Figure 13(a) presents a multitier energy level diagram for the isomerization of conformer A following selective ex-

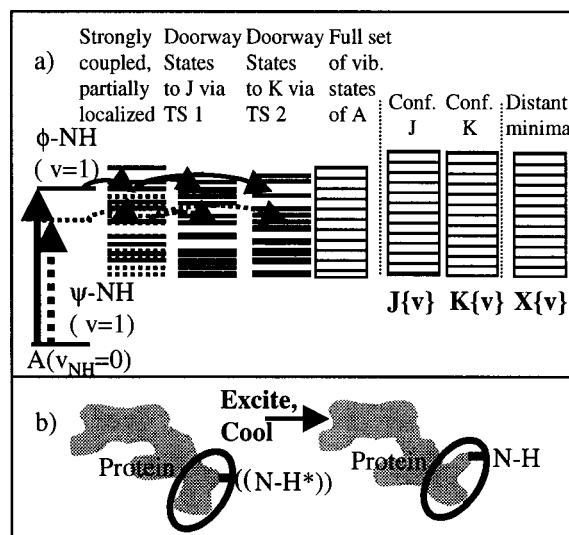


FIG. 13. (a) Schematic energy level diagram containing tiers of vibrational energy levels relevant to conformational isomerization of conformer A following selective IR excitation of either its ϕ -amide or ψ -amide NH stretch fundamental. The arrows indicate state mixing between the tiers of levels, first to a set of strongly coupled, partially localized levels, and then to the doorway states that lead to isomerization via transition state 1 (leading to conformer J) or 2 (leading to conformer K).

citation of either of two NH stretch fundamentals. A first level of distinction among the full set of vibrational states is into tiers of vibrational levels associated with each of the conformational minima of the molecule, as depicted on the right-hand side of the diagram. It seems unlikely that any mode specificity would survive sampling the states associated with a second conformational minimum. As a result, RRKM theory should be able to account for later steps in the isomerization process leading to final products. A description of mode-specific effects could then concentrate on IVR within the vibrational states localized within the well of conformer A, including doorway states that couple strongly to a given isomerization transition state, as shown on the left-hand side of Fig. 13(a).

The makeup of the tiers of levels of conformer A depends to some extent on the properties of the excitation source used. The hole-filling experiment uses nanosecond IR lasers with about 0.2 cm^{-1} resolution for IR excitation. With this excitation source, the entire NH stretch ($\nu=1$) zero-order bright state is not coherently excited. Under these circumstances, the makeup of the states prepared by the laser will reflect a partially “prerelaxed” vibrational distribution of both levels that is difficult to predict from first principles and prevents a simple description in which the energy is initially localized in the NH bond at $t=0$.¹⁰ With this caveat in mind, it is still useful to consider a tier model for the IVR beginning from a localized NH stretch level.

The time scale for loss of the initial XH($\nu=1$) excitation will be dominated by strong coupling to a small number of states, and thus be quite insensitive to the full vibrational density of states, a point driven home by several previous studies.^{11,14,22} The first tier is thus composed of levels that are specific to a given NH($\nu=1$) state (e.g., ψ -NH versus ϕ -NH), being coupled to it by low-order anharmonic terms

in the potential with strong mechanical coupling to the excited NH oscillator (e.g., NH bend overtones). A more refined description could then include successive tiers with increasing delocalization of the vibrational excitation. In a classical description, this is equivalent to saying that energy flows out of the NH stretch in successive steps down the flexible side chain as it spreads out over the entire molecule.²¹

Among the full set of vibrational states of conformer A at the energy of the NH stretch fundamental are those that have significant torsional excitation along coordinates associated with the competing first isomerization steps. These doorway states are pulled out of the full set of vibrational levels in Fig. 13(a) in order to highlight their importance to the mode-specific dynamics.

Mode-specific differences in the isomerization quantum yields would be possible if: (i) the doorway states for A–J and A–K isomerization are different in makeup (i.e., they are themselves somewhat localized in the region of initial vibrational excitation), (ii) coupling of the partially localized states to the doorway states is strong relative to coupling to the full set of vibrational states of A, and (iii) the coupling to the two sets of doorway states is sensitive to which NH mode is initially excited. Under such circumstances, IR excitation initially localized on a given NH oscillator could couple more strongly to states across one barrier, while excitation elsewhere would couple to states along another pathway, producing mode-specific isomerization quantum yields.

Conformation specificity in the quantum yields is somewhat less demanding. Here, IVR can be complete within a given conformational well, but must be incomplete between wells. Then, cooling can steer or arrest the isomerization process in different ways if the isomerization is initiated from different conformational wells via conformation-specific vibrational excitation. This is the limit we observe, at least weakly, in the quantum yields of NATMA and NATA.

D. The role of cooling collisions on the intramolecular dynamics

The intramolecular dynamics occur in concert with the collisional cooling of the vibrationally excited molecule. In our case, this cooling is occurring during the supersonic expansion process. These cooling collisions provide another set of time scales for the experiment: (i) The time between collisions (~100 ps initially), (ii) the time to cooling below the energy where isomerization can occur, and (iii) the time to recool to the zero-point level. In this sense, the present reliance of the experiment on collisional cooling to probe intramolecular dynamics bears some resemblance with the chemical timing experiments of Parmenter and co-workers.^{23–27} The cooling collisions complicate the theoretical modeling of the hole-filling experiment because the temperature and collision frequency are changing as the expansion occurs.

The cooling collisions also influence the IVR process, which is interrupted and redirected as each collision occurs, producing states with vibrational character with each collision. One might anticipate that such collisions will enhance

IVR. However, as Parmenter *et al.*²⁸ has pointed out, high selectivity in state-to-state vibrational energy transfer is more the rule than the exception, even in polyatomic molecules. Unfortunately, the hole-filling experiment is so far incapable of measuring the energy content of the molecules as they cool, but rather gives up such information in favor of collecting the population quantitatively into the zero-point levels for detection. Several groups have used a range of ingenious methods to determine the average energy lost per collision as a function of internal energy for various excited molecules with a range of collision partners in bulb studies.^{28–31} These studies lead to the conclusion that the average internal energy lost per collision scales roughly with the average vibrational energy in the hot donor. Much of that work involved the excitation of much larger amounts of energy by ultraviolet excitation in molecules without significant conformational flexibility. Based on our limited experience to date with the hole-filling experiment, it is clear that molecules, such as NATA and NATMA, are efficiently vibrationally cooled by helium. We ascribe this to the presence of very low-frequency vibrations (~10–20 cm⁻¹) in NATMA and NATA that dominate the vibrational density of states and are efficiently deactivated even by helium collisions. Indole, which lacks such low-frequency vibrations, is not re-cooled into its zero-point level under the same conditions that completely re-cool NATMA and NATA.

Clearly, the observed quantum yields depend to some degree on this cooling rate, since the isomerization pathways are traversed in parallel with vibrational cooling. It would seem important to experimentally control and vary this cooling rate over as wide a range as possible. This is presently being pursued in studies of melatonin, where a greater signal allows us to explore a wider range of cooling conditions.

E. Vibrational mode specificity in the large molecule limit

Finally, it is worth considering how the picture put forward in Fig. 13(a) would extend to much larger molecules. However, instead of couching the argument in the strained language of IVR, it may be helpful to return to a simple classical picture of the experiment in assessing the prospects for influencing the isomerization product yields by exciting different bonds in a large flexible molecule. As shown in Fig. 13(b), in such a large macromolecule (e.g., a protein), it makes good intuitive sense that, if it were possible to excite a local mode vibration (such as an NH stretch), the molecule could use this energy to undergo conformational isomerization near the point of excitation, but that other regions of the protein far from that point would be unaffected by the vibrational excitation. Yu and Leitner²⁰ recently carried out a theoretical analysis of vibrational energy flow in proteins that begins to address these issues. It is still an open question as to whether molecules the sizes of NATMA or NATA are near the cross-over region where such behavior can be observed in hole-filling experiments like those described here.

VII. CONCLUSIONS

This article has described in some detail the experimental methods of IR-UV HFS and its close analog, IR-PTS. These methods show considerable promise for probing the dynamics of conformational isomerization at an unprecedented level of detail, starting from vibrational excitation of single conformations in single vibrational modes. The methods for extracting isomerization quantum yields have been outlined. In NATMA and NATA, these quantum yields show modest conformation selectivity, but only a hint of vibrational mode selectivity. However, further studies of this type are clearly warranted in order to address how the isomerization dynamics depend on the size and degree of flexibility of the molecule. Future studies also need to address the effects of changing the energy of excitation (either by isotopic substitution, overtone excitation, or extension into the midinfrared), varying the rate of cooling over a wider range, and extending the studies to solvent-containing complexes. Several of these aspects are currently being pursued.

ACKNOWLEDGMENTS

The authors gratefully acknowledge the NSF Experimental Physical Chemistry program (CHE0242818) and the Petroleum Research Fund, administered by the American Chemical Society (35988-AC6) for their support of this work. The authors also gratefully acknowledge fruitful discussions with R. W. Field and B. H. Pate on IVR in flexible molecules.

¹G. Gershinsky and E. Pollak, J. Chem. Phys. **107**, 812 (1997).

²J. S. Baskin, L. Banares, S. Pedersen, and A. H. Zewail, J. Phys. Chem. **100**, 11920 (1996).

³J. H. F. V. D. Vachev, B. A. Grishanin, V. N. Zadkov, and N. I. Koroteev, J. Phys. Chem. **99** (15), 5247 (1995).

⁴A. Liwo, P. Arlukowicz, C. Czaplowski, S. Oldziej, J. Pillardy, and H. A. Scheraga, Proc. Natl. Acad. Sci. U.S.A. **99**, 1937 (2002).

⁵Z. Qin, J. Ervin, E. Larios, M. Gruebele, and H. Kihara, J. Phys. Chem. B **106**, 13040 (2002).

⁶B. C. Dian, A. Longarte, and T. S. Zwier, Science **296**, 2369 (2002).

⁷B. C. Dian, A. Longarte, S. Mercier, D. Evans, D. J. Wales, and T. S. Zwier, J. Chem. Phys. **117**, 10688 (2002).

⁸B. C. Dian, A. Longarte, and T. S. Zwier, J. Chem. Phys. **118**, 2696 (2003).

⁹C. W. Garland, J. W. Nibler, and D. P. Shoemaker, *Experiments in Physical Chemistry* (McGraw-Hill, New York, 2003), p. 733.

¹⁰D. A. Evans, D. J. Wales, B. C. Dian, and T. S. Zwier, J. Chem. Phys. **120**, 148 (2004).

¹¹D. J. Nesbitt and R. W. Field, J. Phys. Chem. **100**, 12735 (1996).

¹²M. Gruebele and R. Bigwood, Int. Rev. Phys. Chem. **17**, 91 (1998).

¹³J. Keske, D. A. McWhorter, and B. H. Pate, Int. Rev. Phys. Chem. **19**, 363 (2000).

¹⁴K. K. Lehmann, G. Scoles, and B. H. Pate, Annu. Rev. Phys. Chem. **45**, 241 (1994).

¹⁵C. S. Parmenter and B. M. Stone, J. Chem. Phys. **84**, 4710 (1986).

¹⁶Z. H. Wang, A. Pakoulev, and D. D. Dlott, Science **296**, 2201 (2002).

¹⁷C. G. Elles, D. Bingemann, M. M. Heckscher, and F. F. Crim, J. Chem. Phys. **118**, 5587 (2003).

¹⁸Y. C. Chou, C. L. Huang, I. C. Chen, C. K. Ni, and A. H. Kung, J. Chem. Phys. **117**, 7906 (2002).

¹⁹R. M. Bigwood and M. Gruebele, J. Mol. Struct.: THEOCHEM **589**, 447 (2002).

²⁰O. V. Boyarkin, T. R. Rizzo, and D. S. Perry, J. Chem. Phys. **110**, 11346 (1999).

²¹X. Yu and D. M. Leitner, J. Phys. Chem. B **107**, 1698 (2003).

²²A. McElroy and D. J. Nesbitt, J. Chem. Phys. **92**, 2229 (1990).

²³R. A. Coveleskie, D. A. Dolton, and C. S. Parmenter, J. Phys. Chem. **89**, 645 (1985).

²⁴R. A. Colvelleskie, D. A. Dolton, and C. S. Parmenter, J. Phys. Chem. **89**, 655 (1985).

²⁵K. W. Holtzclaw and C. S. Parmenter, J. Chem. Phys. **84**, 1099 (1986).

²⁶D. A. Dolson, K. W. Holtzclaw, D. B. Moss, and C. S. Parmenter, J. Chem. Phys. **84**, 1119 (1986).

²⁷D. B. Moss and C. S. Parmenter, J. Chem. Phys. **98**, 6897 (1993).

²⁸G. W. Flynn, C. S. Parmenter, and A. M. Wodtke, J. Phys. Chem. **100**, 12817 (1996).

²⁹J. R. Barker, J. Phys. Chem. **88**, 11 (1984).

³⁰J. Troe, Pure Appl. Chem. **69**, 841 (1997).

³¹D. Schwarzer, J. Troe, M. Votsmeier, and M. Zerezke, J. Chem. Phys. **105**, 3121 (1996).